Journal of Laser Applications

RESEARCH ARTICLE | OCTOBER 13 2023

Predictive modeling of lattice structure design for 316L stainless steel using machine learning in the L-PBF process

Special Collection: Proceedings of the International Congress of Applications of Lasers & Electro-Optics (ICALEO 2023)

Karim Asami ; Sebastian Roth ; Michel Krukenberg; Tim Röver ; Dirk Herzog ; Claus Emmelmann

J. Laser Appl. 35, 042046 (2023)
https://doi.org/10.2351/7.0001174

Journal of Laser Applications ARTICLE pubs.aip.org/lia/jla

Predictive modeling of lattice structure design for 316L stainless steel using machine learning in the L-PBF process

Cite as: J. Laser Appl. 35, 042046 (2023); doi: 10.2351/7.0001174
Submitted: 11 July 2023 · Accepted: 27 September 2023 ·
Published Online: 13 October 2023

Karim Asami,[1] Sebastian Roth,[1] Michel Krukenberg,[1] Tim Röver,[1] Dirk Herzog,[2] and Claus Emmelmann[1]

AFFILIATIONS

[1]Institute of Laser and System Technologies (iLAS), Hamburg University of Technology (TUHH), Harburger Schloßstraße 28, 21079 Hamburg, Germany
[2]Institute for Industrialization of Smart Materials (ISM), Hamburg University of Technology (TUHH), Eißendorfer Straße 40, 21073 Hamburg, Germany

Note: Paper published as part of the special topic on Proceedings of the International Congress of Applications of Lasers & Electro-Optics 2023.

ABSTRACT

Lattice structures in additive manufacturing of 316L stainless steel have gained increasing attention due to their well-suited mechanical properties and lightweight characteristics. Infill structures such as honeycomb, lattice, and gyroid have shown promise in achieving desirable mechanical properties for various applications. However, the design process of these structures is complex and time-consuming. In this study, we propose a machine learning-based approach to optimize the design of honeycomb, lattice, and gyroid infill structures in 316L stainless steel fabricated using laser powder bed fusion (L-PBF) technology under different loading conditions. A dataset of simulated lattice structures with varying geometries, wall thickness, distance, and angle using a computational model that simulates the mechanical behavior of infill structures under different loading conditions was generated. The dataset was then used to train a machine learning model to predict the mechanical properties of infill structures based on their design parameters. Using the trained machine learning model, we then performed a design exploration to identify the optimal infill structure geometry for a given set of mechanical requirements and loading conditions. Finally, we fabricated the optimized infill structures using L-PBF technology and conducted a series of mechanical tests to validate their performance under different loading conditions. Overall, our study demonstrates the potential of machine learning-based approaches for efficient and effective designing of honeycomb, lattice, and gyroid infill structures in 316L stainless steel fabricated using L-PBF technology under different loading conditions. Furthermore, this approach can be used for dynamic loading studies of infill structures.

Key words: Additive manufacturing, machine learning, DfAM, lattice structures, L-PBF, finite element method, simulation, 316L

I. INTRODUCTION

Additive manufacturing (AM according to ISO/ASTM 52900:2015[1]) has emerged as a promising technology to produce complex components with a variety of benefits and specific attributes, e.g., low thermal conductivity and tailor-made mechanical properties.[2–4] One of the key challenges is to reduce the production time while ensuring the structural integrity of the part. So far, additive manufacturing has primarily been used for prototype manufacturing and small-scale fabrication.[5] Usually, an experimental design setup is required to reduce the time effort and investigation of specific process parameter and the characteristics of the final part.[6,7] Laser powder bed fusion (L-PBF) technology is the most widely used additive manufacturing process due to its high process stability and repeatable manufacturing accuracy.[8]

However, one solution for the reduction of manufacturing time is the use of infill structures by lattices, which can be applied in areas with lower component utilization and has been already excessively investigated for the L-PBF process.[9–11] These infill structures make it possible to reduce material waste and optimize part weight without compromising the outer contour and material thickness at the stress points.

Infill structures are used in a variety of areas, including mold making, replacement part, and automotive and aerospace applications.[12] For example, in mold making, infill structures can help reduce material waste by filling the cavity inside the part with a lattice structure that has the same outer contour as the original part. This allows efficient use of material while reducing part weight. For instance, in replacement part applications, infill structures can help maintain part performance and function while reducing weight and manufacturing costs.

Owing to the large number of process parameters,[13] machine time, and pre- and postprocess effort, a complete experimental investigation of the large number of different types of infill structures[9] is inefficient. Therefore, simulations based on numerical methods such as finite elements are predominantly used for the investigation of process parameters and characteristic structural properties.[14,15]

Successful manufacturing in the L-PBF process requires experienced designers for the part development with different features, for manufacturing with the process parameters and part orientation, and for postprocessing. In order to avoid multiple trial and error iterations for a product, the design of experiments and simulations, which depend on the computational accuracy and effort, design guidelines for different part features depending on the process and material are developed to ensure successful part production.[16–18]

Machine learning (ML) approaches have been increasingly applied for design aspects in additive manufacturing technologies over recent years to predict the desired component properties as a function of process parameters.[19] For example, ML for the design features has been previously used for roughness prediction of surfaces using regression algorithms,[20] density and melt pool prediction with regression algorithms,[21] and prediction of mechanical properties also applying regression algorithms.[22] Furthermore, a Gaussian-based ML model was used to optimize the process parameters and predict the remelt depth of tracks as a function of the combined laser power and laser scan speed in the L-PBF process.[23,24] For the postprocess, there exists also an optical-based ML model where the data are provided to support vector machine (SVM) classifiers to predict density regions of the part.[25]

There exists an approach that predicts the printability of specific voxel-based infill structure designs using convolutional neural networks (CNNs) as well as neural networks (NNs) for fabrication and, thus, prevents failure during manufacturing.[26] Due to the voxelization size and the hybrid ML architecture, a very high computational time is required, and thus, the efficiency is very limited. This research gap presents the potential for the development of a machine learning model that successfully captures the complex relationships between infill structures and stress with low computational effort, enabling the prediction of the optimal design for infill structures.

With the aid of the ML algorithm, the optimum infill structure with its geometric properties (orientation, wall thickness, etc.) can be determined on the basis of known load conditions, resulting in material and production time savings. Furthermore, this approach can ensure the load-dependent first time right production, as the designs in the algorithm are considered to be manufacturable and can, thus, serve as a complement to existing guidelines. Therefore, this approach contributes one fundamental for the AI-based design for additive manufacturing (DfAM) with unknown design feature combinations that often occur in AM.[16–18]

This investigation explores the potential of machine learning and outlines a possible approach for developing a model that predict stress values based on simulated and experimental performed datasets.

II. MATERIALS AND METHODS

Figure 1 illustrates the methodology used in this paper. For the development of the ML model, parametric designs of infill geometries were initially generated. These infill designs were varied using the parameters displayed in Fig. 1 and simulated with different loading conditions with the aim of determining the maximum stress that occurs in the component. The parameters shown in blue were used as training and test parameters for the ML model. The results of the stress were obtained by compression and 3-point bending tests according to Refs. 27 and 28.

A. Specimen design

The design development of infill structures focuses on grid, gyroid, and honeycomb structures, which were analyzed mainly in the L-PBF process for lightweight application.[29] For the specimen design modeling, cylindrical bars and rectangular beams were considered as basic geometries used in different design applications as particular features. The dimension of cylindrical rods is 40 mm in diameter and height. The rectangular beams have a dimension of

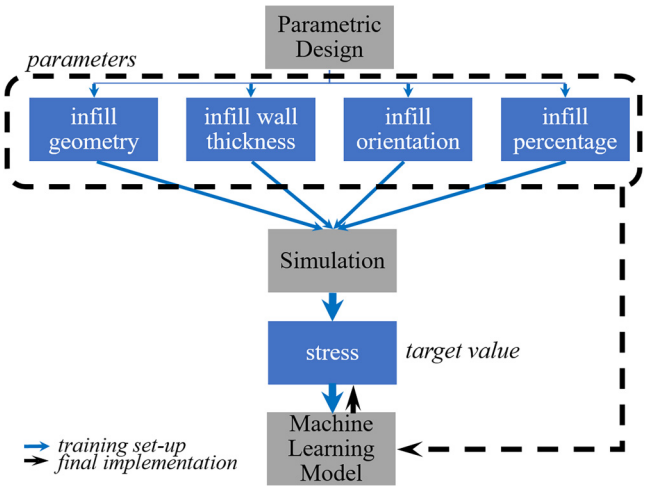

FIG. 1. Methodology for ML model development and stress prediction.

TABLE I. Specimen load and infill parameter variation.

Parameter	Unit	 Cylindrical rod	 Rectangular beam
Infill type	—	Grid and honeycomb	Grid, honeycomb, and gyroid
Wall thickness	mm	1, 2, 4, 6, 8, and 10	0.5, 1, 2, 4, 6, and 8
Infill orientation	deg	0, 15, 30, 45, 60, 75, and 90	0, 15, 30, 45, 60, 75, and 90
Infill percentage	%	10, 20, … , 100	10, 20, … , 100
Load	kN	50, 100, and 200	10 and 20

80 mm in length and a square edge length of 20 mm. Also the size of the rectangular beams has been varied to a reduced length of 50 mm for manufacturable reasons. The honeycomb and lattice structures were modeled with 3D-CAD software *Autodesk inventor* (Autodesk, San Francisco, USA), and the gyroid structures were designed with *nTopolgy* (nTopology, New York City, USA). Table I presents the different variations in the infill parameters and loads. A total of 167 different samples have been designed with each parameter combination.

For the validation of the simulation, four different beams were manufactured from different variations using the L-PBF method. Two of the samples are gyroid structures with 60% and 80% infill, and one sample each is a lattice and honeycomb structure with 60% infill and 1 mm wall thickness. The specimens were produced on the OCM MPrint (One Click Metal, Tamm, Germany), and the material that was made of is the widely used AISI 316L (1.4404) powder that is also provided by the manufacturer (see Table II), which is used in versatile applications in different fields.[18] Figure 2 shows powder characterization provided by the manufacturer. The particles are mainly spherical with occasional elliptic necks. The particle size distribution is $D_{10} = 19\,\mu$m, $D_{50} = 29\,\mu$m, and $D90 = 43\,\mu$m according to ISO 13322-2.[30]

For the manufacturing of the specimen, the following process parameter was chosen: the laser diameter of 70 μm, the laser power of 200 W, the scan speed of 800 mm/s, and the layer thickness of 40 μm.

Figure 3 illustrates the different manufactured components for the 3-point bending tests.

The 3-point bending tests were performed with the specimens. The machine used is the Zwick/Roell Z010 (Zwick Roell Group, Ulm, Germany), and the force was recorded over time and displacement. All samples were heat treated for 1 h at 900 °C in an Oven ExSO90 by the manufacturer Aim3D (Aim3D GmbH, Rostock, Germany) according to Ref. 31 to reduce thermal stress peaks due to the manufacturing process.

TABLE II. Composition of the elements for 316L powder (Ref. 30).

Element	C	Si	Mn	Cr	Ni	Mo	Fe
wt. %	0.03	1	>2	16–18	11–14	2–3	Basis

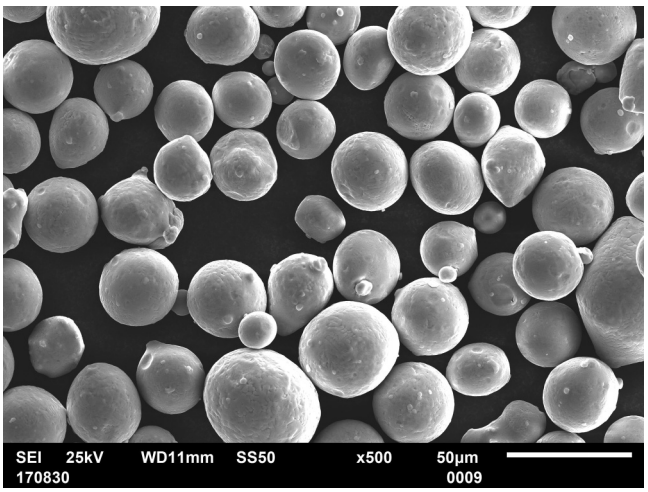

FIG. 2. Illustration of the particle distribution (Ref. 30).

B. Simulation

The pressure and 3-point bending simulations according to Refs. 27 and 28 were performed in *Altair Hyperworks 2021* (Altair, Michigan, USA). A convergence study has been performed in a way that a trade-off between iteration steps and computation time has been selected as the target. The cylindrical bars have been used for compression simulations and the rectangular beams for bending tests. For the cylindrical specimen, tetra-elements with four nodes were used as a mesh. The rectangular beams have been designed for the mesh with tetrahedra and pyramid elements. Simulation was performed for each sample by varying the geometry features and the load condition. The maximum stress for each

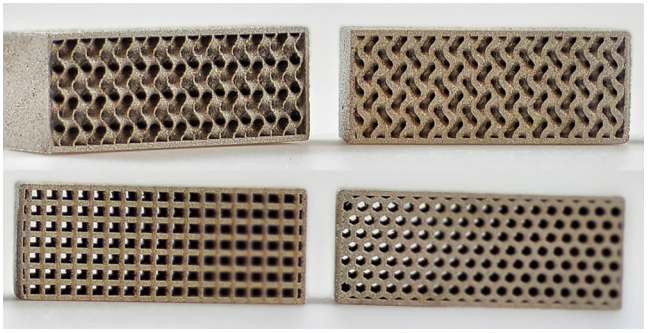

FIG. 3. Manufactured specimens of different investigated types of infill: 60% gyroid (top left), 80% gyroid (top right), 60% grid (bottom left), and 60% honeycomb structure (bottom right).

TABLE III. Assumed material properties.

Element type	Tetra, tetrahedra, and pyramid
Element size	0.01–2 (mm)
Young's modulus	200 (GPa)
Density	7.9 (g/cm^3)
Poisson's ratio	0.27

variation was considered as the target value. The material chosen for the simulation is AISI 316L stainless steel. Table III shows the material properties assumed for the simulations.

In Fig. 4, the simulation approach with different element types is depicted. It is assumed that the force does not impact on a point but on a surface, as in the reality of the tests.

III. MACHINE LEARNING

The machine learning approach for predicting target variables is based on a supervised learning procedure. Regression models are used to model the relationship between the input data and the target variables. In this paper, four specific regression models are considered: decision tree regression (DTR), linear regression (LR), random forest regressor (RFR), and gradient boosting regression (GBR). The 167 simulated compression and 3-point bending test variations of the infill geometries serve as the data basis for the algorithms. The implementation of different models has been performed in PYTHON 3.8. Mainly PANDAS and SCIKIT-learn have been applied for the creation of ML models.[32] The datasets were divided into training and test data for the prediction by different models. Out of the 167 datasets, 70% were allocated to the training data and 30% to the test data. A main criterion for the statement of accuracy for regression-based models is the mean squared error (MSE), which is also applied in this analysis.[21] Another criterion for the accuracy of the models is the consideration of the R^2-score also influenced by the MSE value and examined here.[32] The comparison of the models is done by the normalized values of the variations; thus, the impact of the values occur in sizes from 0 to 1. Finally, predictions are presented for the stresses across the devised loads and different characteristics of the infill structures.

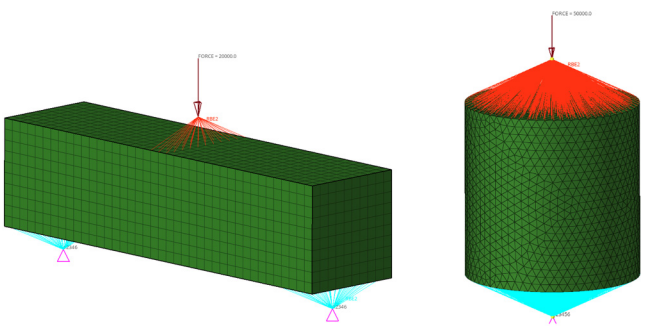

FIG. 4. Compression and 3-point bending simulation with tetra elements (right) and the combination of pyramid and tetrahedra elements (left).

IV. RESULT AND DISCUSSION

All simulations could be executed and the maximum stress could be identified. Depending on the variations, the maximum stresses are in the range from 43.56 MPa (external load of 50 kN, infill of 100%, honeycomb structure, wall thickness of 1 mm, and orientation of 0°) for compression simulation to 1121.35 MPa (external load of 20 kN, infill of 10%, honeycomb structure, wall thickness of 1 mm, and orientation of 0°) for 3-point bending simulation. It is obvious that the 1121.35 MPa maximum stress is higher than the tensile strength of the material with 574 MPa.[30] Nevertheless, these values are considered for qualitative statements about the prediction accuracy of the model. As expected, the maximum stresses increase primarily with increasing load and decreasing percent infill for each orientation and structure. A comparison with other pressure simulations for honeycomb structures shows a comparable stress distribution. It should be mentioned that this comparison is only qualitatively possible, because, on the one hand, unit cells without an external shell were constructed for the simulation and, on the other hand, lower loads were assumed.[10,29] Figure 5 shows the stress

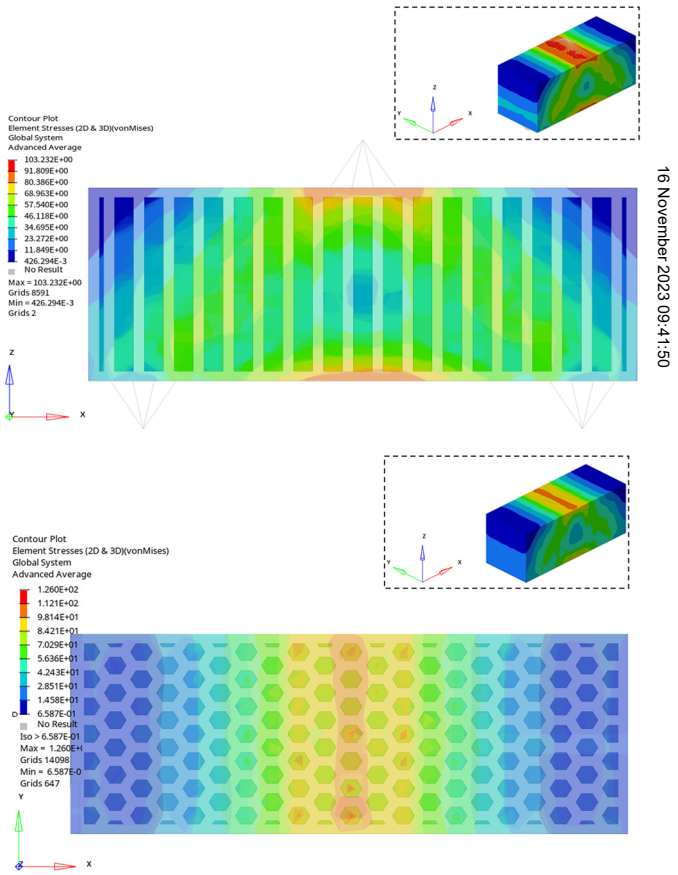

FIG. 5. Stress distribution of the 3-point bending simulation at a load of 10 kN for the bending beams with grid (side view, top image) and honeycomb structure (top view, bottom image).

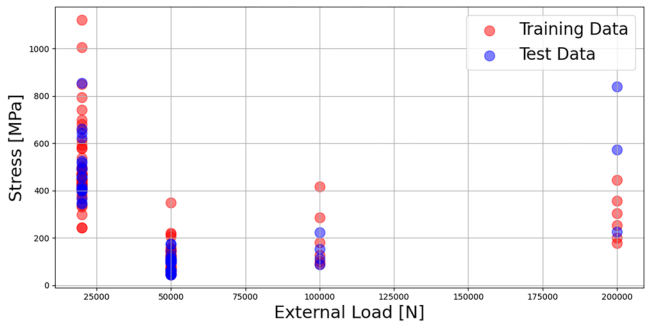

FIG. 6. Distribution of simulated stresses in test and training data.

distribution of the 3-point bending simulation at a load of 10 kN representative for grid (top) and honeycomb (bottom) structures with a length of 50 and 20 mm per edge strand in cross section. It can be observed that the maximum stress in both cases occurs at the point of force application and decreases with increasing distance in all spatial directions. The maximum stress is 103.23 MPa for the grid structure and 125.98 MPa for the honeycomb structure. The prepared samples for the experimental study were performed with the same experimental setup. At a bending load of 10 kN, the lattice specimen has been displaced 1.02 mm in the z-direction at the force application point. The simulation shows a displacement of 1.5 mm at the same point. This difference is due to approximation of the simulation and is within the acceptable range. The displacement of the honeycomb structures is 1.6 mm in the simulation and 0.99 mm in the experimental test. The difference is slightly larger here. The displacement of the gyroid infill structure with 80% indicated a displacement with 1.2 mm, a larger plastoelastic deformation. The gyroid infill structure with 60% infill plastically deformed at the load of 10 kN, which could be correctly actuated by the simulation with a higher maximum stress than the tensile strength. The deformation in this case is 4.72 mm.

The maximum stresses of different configurations were divided into training and test data (see Fig. 6). This figure depicts the maximum stress across the external applied load. The training data shown in red have a share of 70% and the test data in blue have a share of 30%. It can be observed that the test data are barely represented at 200 kN. Due to the small dataset and big jumps in the input data, cross-validation of the data has been performed to avoid overfitting using k-1 folds ($k = 5$) for the training data and onefold for the test data. The number of repeats is 10.

Figure 7 displays the predictions (y-axis) on the simulated data (x-axis) for four different models: LR, DTR, GBR, and RFR for the test data. The red lines indicate the point where the predictions coincide with the simulated data. It is obvious that the points

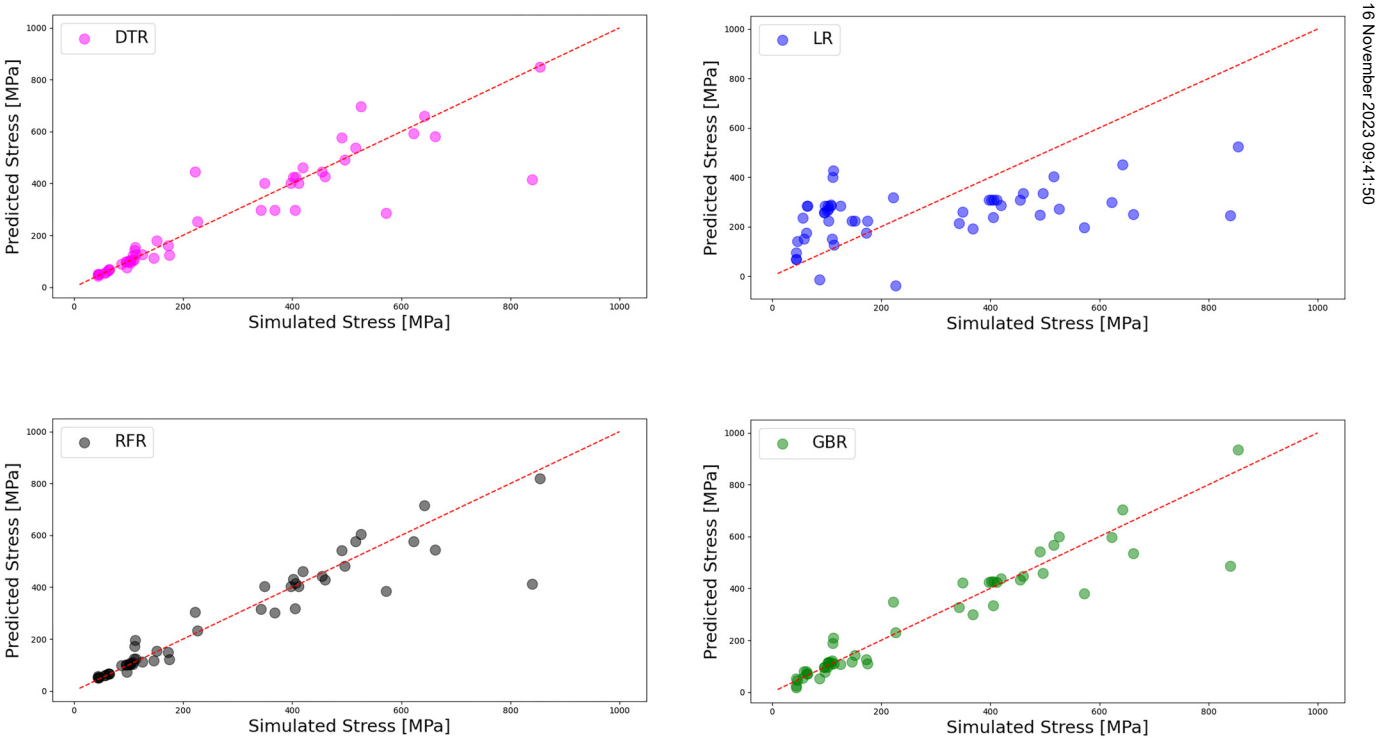

FIG. 7. Stress prediction as a function of simulated stress for different models linear regression (LR, blue, top left), decision tree regression (DTR, magenta, top right), gradient boost regression (GBR, green, bottom left), and random forest regression (RFR, gray, bottom right).

on the red line, therefore, accurately predict the simulations. It should be mentioned that with increasing distance to the red line, the predictions are less accurate. Since the test data are only available for 20, 50, and 100 kN load cases, a gap between low and high stress regions can be recognized in all diagrams. The LR model makes an accurate prediction in only one case. All other points deviate strongly from the actual values. Therefore, it can be assumed that there is no linear correlation between the input and output parameters. The decision tree model (DTR), in comparison, performs more accurate predictions for lower stresses and underestimates higher stresses. Also, several outliers can be identified in the mid-stress area and just one outlier in the maximum high area. The approximation is acceptable only in the range from 50 to 150 MPa and 400 to 450 MPa. The gradient boost regression (GBR) model also shows a higher approximation accuracy than the LR model but overestimates the stresses for smaller as well as larger loads. Furthermore, it can be observed that in the range of lower stresses, the scatter of the predictions is larger than with the DTR model. In the range above 300 MPa, the deviations of the predictions are smaller compared to the DTR model. Likewise, for large stress, underestimation and overestimation of the simulated stress are apparent. The RFR model shows isolated deviations in the prediction at small and large stresses. In the area of small stresses as in the GBR model, the stresses are increasingly overestimated. This model also has an underestimated prediction for very large stresses (>600 MPa), but it is more accurate than DTR and GBR models. Finally, based on the model comparison, it can be said that LR is unsuitable with the given input parameters, since there is too large scatter independency of the load. The models DTR, GBR, and RFR show a comparably high accuracy in the prediction, whereas the GBR model predicts most frequently.

To examine the trained models for their influencing factors, the data were normalized and the Pearson correlation coefficient was compared. This coefficient is calculated from the variations in the input variables and the output variable.[21] Table IV plots the linear correlations of the input and output variables for different models. It can be recognized that the strongest correlation between load and stress is present for all models. The values vary between 0.716 and 0.723. The second strong dependence is between percent infill and stress at 0.24 for all models. This is plausible since the stress is defined by force per area and, thus, depends directly on both input parameters. The input variables of wall thickness and orientation show comparatively low correlation with stress for all three models, which are in the interval of 0.014 and 0.020, respectively. In this context, the volume percentage of the infill is more decisive than the other parameters. Infill geometry has the lowest correlation to the target stress with values ranging from 0.004 to 0.009 for all models. This is due to the training data, since the maximum stresses of the simulations and the experimental investigations always occurred at the outer contour, and therefore, the infill geometry played an insignificant role in this context.

The evaluation of the trained models is done by considering the root mean square error (RMSE) and the R^2 parameter. RMSE and R^2 are defined as[33]

$$\mathrm{RMSE}(y, \tilde{y}) = \sqrt{\frac{1}{n}\sum_{i=0}^{n-1}(y_i - \tilde{y}_i)^2}, \tag{1}$$

$$R^2 = 1 - \frac{\sum_{i=1}^{n}(y_i - \tilde{y}_i)^2}{\sum_{i=1}^{n}(y_i - \hat{y})^2}. \tag{2}$$

In this case, y_i is the ith prediction, n is the number of simulations, and $\tilde{y}_i$ is the objective quantity and $\hat{y}$ are the average values of y. The R^2 is a variance-based measure of how well the data of a model fit in percentage. In addition, the RMSE has been taken into account to track the extent of difference between the individual predictions.[33] Table V shows the RMSE and R^2 values for the test data of different models. As already observed from Fig. 7, the LR model has a high deviation in the prediction. This is also confirmed by the RMSE of 197.1 MPa, which is unsuitable for robust prediction. The smallest root mean squared error is found in the GBR model. Therefore, it can be assumed that this model can make most accurate predictions. The RFR model has a slightly higher root mean square error than the GBR model, but it is less than 10 MPa. Therefore, this model also indicates comparable prediction accuracy. The DTR model has 86.67 MPa for the test data, a larger error than the RFR and GBR models; however, both errors are in the same order of magnitude (smaller than 100 MPa). The GBR model shows the smallest error and, thus, the highest robustness and flexibility which was previously recognized in Ref. 21. The assumption that the models are overfitted due to a small dataset could not be confirmed although a high deviation in the RMSE would have been an indicator. Attempts to distribute training and test data differently, such as 80% training and 20% test data, resulted in no significantly lower RMSE. The difference in RSME is here for all models less than 8 MPa. The reason for the deviation in the error is apparently due to the large distribution of the variation parameters and, thus, by the small number of simulated data. A larger database and the processing of the available data should significantly reduce the mean squared error. The overfitting can also be excluded by means of the R^2 score because none of the

TABLE IV. Correlation of the input variables of different models, GBR, RFR, and DTR, for stress as the target parameter.

Model	Load	Infill geometry	Wall thickness	Infill orientation	Infill percentage
GBR	0.723	0.004	0.017	0.015	0.24
RFR	0.719	0.008	0.020	0.014	0.24
DTR	0.716	0.009	0.014	0.018	0.24

TABLE V. Mean square error for the test data (MPa) and R^2 (–) score for the investigated models GBR, RFR, DTR, and LR.

Model	Average RMSE (MPa)	R^2
GBR	67.31	0.91
RFR	77.07	0.88
DTR	86.67	0.84
LR	197.1	0.20

models reaches the value 1.[33] The R^2 value for the LR model displays a value of about 0.20, which by definition is weak. Hence, this is another indication that there is no linear relation between the variations and the target quantity. The models GRB, RFR, and DTR show for R^2 with 0.84– 0.91 a high proportion of independent variables that can be described with the variance of dependent variables. As overfitting of the models could be excluded, all three models seem to be suitable for stress prediction. Ultimately, a larger database may result in a lower squared error and a greater difference in the RMSE of various model accuracies.

Finally, new predictions for previously unknown parameter variations of infill and load have been performed to classify the results. The external load has been assumed to be 10–100 kN in 10 kN steps. A 60% infill volume fraction was assumed for all specimens. The infill structures used are gyroid, grid, and honeycomb, respectively. The wall thickness alternates between 1 and 2 mm and the orientation between 0° and 90°.

Figure 8 below shows the stress predictions of the varied assumed input variables for all four models investigated. It can be recognized that all four models also make a prediction for unknown parameter variations. The LR model deviates significantly in stress prediction from the other models for the all loads, demonstrating again the unsuitability for this approach. The DTR, GBR, and RFR models predict similar stress values for the 50 kN load. These are approximately 60 MPa. The deviations are larger for the prediction at 30 and 10 kN, which are explained in Fig. 7. For smaller loads, the DTR, RFR, and GBR models overestimate and underestimate the simulated stresses, respectively. The predicted stresses for the 10 kN load at GBR are approximately 430 MPa for the honeycomb structure and around 425 MPa for the grid structure. The DTR model predicts 410 MPa for honeycomb and 404 MPa for grid structures. The RFR model predicts 409 MPa for the honeycomb structure and 401 MPa for the grid structure. A comparison with Fig. 7 shows that all models predict a deviation from the simulated stresses that can be explained by the mean square errors, and the data basis is not yet sufficient. Nevertheless, all three models predict qualitatively correctly that the grid structures have a lower maximum stress at a load of 10 kN than the honeycomb structures.

The results of this study demonstrate that various ML algorithms DTR, GRB, and RFR are basically able to make maximum stress predictions for a variety of loads and infill parameters. Furthermore, the investigations could show that some models are more suitable than others for the prediction of stresses depending on the infill parameters and loading situation. Nevertheless, it has also been clearly recognized that the number of data for the development of such an ML algorithm should be significantly larger in order to perform accurate predictions for unknown parameter combination. Nevertheless, the root mean squared error is relatively small at 67.31 MPa for the GBR model. Furthermore, it has been recognized that for the maximum stress in a component with a shell, the volume fraction of the infill is much more dependent than the type and shape of the infill structure. As expected, the GBR model made the most accurate and robust predictions followed by the RFR model. It is obvious that the model prediction is limited to the geometry of the specimens as well as to the use of the AISI 316L material. In order for this model to be more robust in predicting the different infill structures, the stress distribution has to be added to the dataset. Then, areas can be identified in which the different geometric characteristics can be considered more efficiently. Graduated structural combinations are then also predictable.

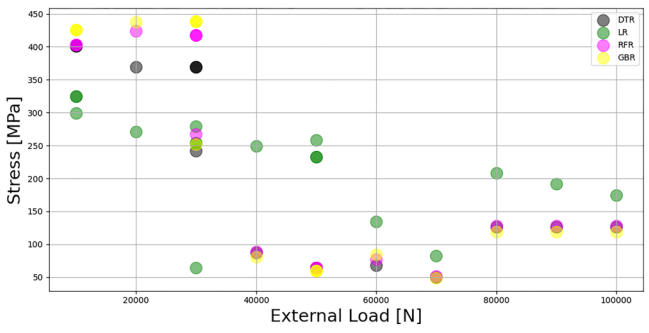

FIG. 8. Stress prediction for unknown parameter variation with ML models DTR, LR, RFR, and GBR.

V. CONCLUSION

In this work, an ML algorithm was developed, which can predict maximum stresses occurring based on the given load and infill parameters of wall thickness, orientation, shape, and volume fraction for the widely used authensitic stainless steel AISI 316L. Bending beams and cylindrical compression specimens with different parameters of the infill structures such as grid, honeycomb, and gyroid were designed, and 167 compression and bending simulations were performed. For experimental validation, four beams with gyroid, honeycomb, and grid structures were fabricated and tested in the L-PBF process. The 167 datasets were then used for testing and training the developed ML algorithm with DTR, GBR, RFR, and LR models. The LR model was found to be unsuitable for this approach. Furthermore, it was shown that the RFR, GBR, and DTR models can make maximum stress predictions with a small relative error. To improve the accuracy, more data are needed for testing and training. It was also concluded that the 70% to 30% split of the training and test data is suitable for this approach. An overfitting of the models could be excluded by the analysis of the R^2 score and the different splitting of the training and test data. In addition, it was validated that a comparison of infill geometries for maximum stresses is only useful if the components have no outer shell. In other cases, the maximum stress occurs directly in the shell in the area of the force application point. In the future, more data will be simulated and validated experimentally in order to improve the accuracy of the ML algorithm and to be able to make quantitative statements for the stress distribution. The stress distribution in the entire component will also be used as a data basis in order to generate a greater influence of various geometric properties of the infill. The aim of this work was to analyze different regression models based on maximum stress, and it was found that one regression model (LR) is unsuitable for stress prediction. In the future, different models such as CNN and deep neural network will be investigated for comparison.[19] These extensions also allow the identification of areas in a component where a certain structure is

more efficient than another in order to be capable of evaluating graduated structures. In that way, a more comprehensive contribution to the DfAM is provided; in that, specific parameter combinations can be evaluated from the stress distribution even before they have been designed or simulated.

AUTHOR DECLARATIONS

Conflict of Interest

The authors have no conflicts to disclose.

Author Contributions

Karim Asami: Conceptualization (lead); Data curation (lead); Investigation (lead); Methodology (lead); Project administration (lead); Software (lead); Validation (lead); Visualization (lead); Writing – original draft (lead); Writing – review & editing (lead). **Sebastian Roth:** Investigation (supporting). **Michel Krukenberg:** Visualization (supporting). **Tim Röver:** Conceptualization (supporting). **Dirk Herzog:** Methodology (supporting). **Claus Emmelmann:** Supervision (supporting).

REFERENCES

[1]ASTM, ISO/ASTM 52900:2015(E) Standard Terminology for Additive Manufacturing—General Principles—Terminology (2015).
[2]M. Zhao, F. Liu, G. Fu, D. Z. Zhang, T. Zhang, and H. Zhou, "Improved mechanical properties and energy absorption of BCC lattice structures with triply periodic minimal surfaces fabricated by SLM," Materials **11**, 2411 (2018).
[3]Chunze Yan, Liang Hao, Ahmed Hussein, Simon Lawrence Bubb, Philippe Young, and David Raymont, "Evaluation of light-weight AlSi10Mg periodic cellular lattice structures fabricated via direct metal laser sintering," J. Mater. Process. Technol. **214**, 856–864 (2014).
[4]M. Smith, Z. Guan, and W. J. Cantwell, "Finite element modelling of the compressive response of lattice structures manufactured using the selective laser melting technique," Int. J. Mech. Sci. **67**, 28–41 (2013).
[5]T. Wohlers, R. I. Campbell, O. Diegel, R. Huff, and J. Kowen, *Wohlers Report 2019: 3D Printing and Additive Manufacturing State of the Industry* (Wohlers Associates, Fort Collins, CO, 2019).
[6]J. J. S. Dilip *et al.*, "Influence of processing parameters on the evolution of melt pool, porosity, and microstructures in Ti-6Al-4V alloy parts fabricated by selective laser melting," Prog. Addit. Manuf. **2**, 157–167 (2017).
[7]M. Elsayed, M. Ghazy, Y. Youssef, and K. Essa, "Optimization of SLM process parameters for Ti6Al4 V medical implants," Rapid Prototyp. J. **25**, 433–447 (2019).
[8]K. Bartsch, D. Herzog, B. Bossen, and C. Emmelmann, "Material modeling of Ti–6Al–4 V alloy processed by laser powder bed fusion for application in macroscale process simulation," Mater. Sci. Eng. A **814**, 141237 (2021).
[9]A. Seharing, A. H. Azman, and S. Abdullah, "A review on integration of lightweight gradient lattice structures in additive manufacturing parts," Adv. Mech. Eng. **12**, 168781402091695 (2020).
[10]Q. Zhang, W. Wu, and J. Liu, "Local strengthening design and compressive behavior study of the triangular honeycomb structure," Metals **12**, 1779 (2022).
[11]T. Rosnitschek, A. Seefeldt, B. Alber-Laukant, T. Neumeyer, V. Altstädt, and S. Tremmel, "Correlations of geometry and infill degree of extrusion additively manufactured 316L stainless steel components," Materials **14**, 5173 (2021).
[12]A. J. Pinkerton, "[INVITED] Lasers in additive manufacturing," Opt. Laser Technol. **78**, 25–32 (2016).
[13]T. G. Spears and S. A. Gold, "In-process sensing in selective laser melting (SLM) additive manufacturing," Integr. Mater. Manuf. Innov. **5**, 16–40 (2016).
[14]M. J. Ansari, D.-S. Nguyen, and H. S. Park, "Investigation of SLM process in terms of temperature distribution and melting pool size: Modeling and experimental approaches," Materials **12**, 1272 (2019).
[15]T. Goldmann, W.-C. Huang, S. Rzepa, J. Džugan, R. Sedláček, and M. Daniel, "Additive manufacturing of honeycomb lattice structure-from theoretical models to polymer and metal products," Materials **15**, 1838 (2022).
[16]K. Asami, K. Bartsch, and C. Emmelmann, "Design rule for efficient support connection point spacing in laser powder bed fusion of Ti6Al4V," in *Proceedings of the 17th Rapid Tech 3D Conference, Erfurt, Germany, 22–23 June 2021*, edited by M. Kynast, G. Witt, and M. Eichmann (Carl Hanser Verlag GmbH & Co. KG, München, 2021), pp. 80–88.
[17]D. Herzog *et al.*, "Design guidelines for laser powder bed fusion in Inconel 718," J. Laser Appl. **34**, 012015 (2022).
[18]K. Asami, D. Herzog, B. Bossen, L. Geyer, C. Klemp, and C. Emmelmann, "Design guidelines for green parts manufactured with stainless steel in the filament based material extrusion process for metals (MEX/M)," in *World PM2022 Proceedings, Lyon, France, 9–13 October 2022* (European Powder Metallurgy Association, Chantilly, France, 2022).
[19]J. Jiang, Y. Xiong, Z. Zhang, and D. W. Rosen, "Machine learning integrated design for additive manufacturing," J. Intell. Manuf. **33**, 1073–1086 (2022).
[20]Z. Li, Z. Zhang, J. Shi, and D. Wu, "Prediction of surface roughness in extrusion-based additive manufacturing with machine learning," Robot. Comput. Integr. Manuf. **57**, 488–495 (2019).
[21]M. Kuehne, K. Bartsch, B. Bossen, and C. Emmelmann, "Predicting melt track geometry and part density in laser powder bed fusion of metals using machine learning," Prog. Addit. Manuf. **8**, 47–54 (2023).
[22]I. Baturynska, "Application of machine learning techniques to predict the mechanical properties of polyamide 2200 (PA12) in additive manufacturing," Appl. Sci. **9**, 1060 (2019).
[23]G. Tapia, S. Khairallah, M. Matthews, W. E. King, and A. Elwany, "Gaussian process-based surrogate modeling framework for process planning in laser powder-bed fusion additive manufacturing of 316L stainless steel," Int. J. Adv. Manuf. Technol. **94**, 3591–3603 (2018).
[24]L. Meng and J. Zhang, "Process design of laser powder bed fusion of stainless steel using a Gaussian process-based machine learning model," JOM **72**, 420–428 (2020).
[25]W. Zouhri *et al.*, "Characterization of laser powder bed fusion (L-PBF) process quality: A novel approach based on statistical features extraction and support vector machine," Procedia CIRP **99**, 319–324 (2021).
[26]Y. Zhang, S. Yang, G. Dong, and Y. F. Zhao, "Predictive manufacturability assessment system for laser powder bed fusion based on a hybrid machine learning model," Addit. Manuf. **41**, 101946 (2021).
[27]See https://www.astm.org/e0009-09.html for "Standard test methods of compression testing of metallic materials at room temperature," ASTM E9-09, Jan. 2018 [Online].
[28]See https://www.iso.org/standard/72187.html for "Bend test," ISO 7438:2020 Metallic materials [Online].
[29]Tobias Maconachie *et al.*, "SLM lattice structures: Properties, performance, applications and challenges," Mater. Des. **183**, 108137 (2019).
[30]See https://www.metals4printing.com/ for "Technical data sheet m4p™ 316 l," m4p material solutions GmbH, Austria [Online].
[31]M. Sprengel *et al.*, "Towards the optimization of post-laser powder bed fusion stress-relieve treatments of stainless steel 316L," Metall. Mater. Trans. A **52**, 5342–5356 (2021).
[32]F. Pedregosa *et al.*, "Scikit-learn: Machine learning in Python," J. Mach. Learn. Res. **12**, 2825–2830 (2011).
[33]F. Bodendorf and J. Franke, "A machine learning approach to estimate product costs in the early product design phase: A use case from the automotive industry," Procedia CIRP **100**, 643–648 (2021).